Lattice-Boltzmann scheme for dendritic growth in presence of convection

Dmitry Medvedev[*], Klaus Kassner

Otto-von-Guericke-University Magdeburg, Postfach 4120, Magdeburg D-39016, Germany

Abstract

A composite phase-field/lattice-Boltzmann scheme is proposed to simulate dendritic growth from a supercooled melt. The phase change part of the problem is modelled by the phase-field approach of Karma and Rappel, whereas the flow of the liquid is simulated by the lattice-Boltzmann-BGK (LBGK) method into which interactions with solid and thermal convection are incorporated.

Test simulations were performed without convection. The resulting tip velocity, radius and branch pattern were the same as in the finite-difference method of Karma and Rappel. Depending on the level of anisotropy and undercooling, dendrites or doublons were obtained in simulations. Dendritic growth in a shear flow was simulated for different flow velocities as well as the growth in presence of natural thermal convection with different orientations of the crystal in the gravitational field. The influence of parallel flow on the operating state of the tip of the dendrite was investigated.

© 2004 Published by Elsevier B.V.

1. Introduction

Dendrites are common patterns in the solidification of melt. They influence the microstructure and mechanical properties of materials obtained in casting. Therefore, a better understanding of dendritic growth is an important theoretical and practical problem.

Under normal growth conditions, i.e., if we do not have a microgravity setup, the inhomogenous temperature distribution in the solidification sample will inevitably lead to thermal convection. Even under microgravity, the density difference between the two phases will induce convection. Convective flows can substantially influence the

*Corresponding author. Fax: +49 0391 6711205.

E-mail address: dmitry.medvedev@physik.uni-magdeburg.de (D. Medvedev).

growth process and the features of the resulting pattern.

The phase-field method is widely used in simulations of dendritic solidification (e.g. Ref. [1]). Its main advantage is the absence of the necessity of tracking the interface, together with the possibility of keeping good accuracy at moderate computational cost.

The lattice Boltzmann (LB) method is presently a well-established tool to simulate fluid flows, especially flows in complex geometries [2]. It can be easily modified to account for the thermal transport due to convection and diffusion, and buoyancy forces can also be easily incorporated. Other advantages of the method are its good stability and ease of parallelization.

Therefore, it seems natural to combine phase-field and LB approaches for simulations of dendritic growth in external flows. The first attempt in this direction was made in Refs. [3–5]. Our model is similar, but it is simpler in the LB part (at least in 2D) and more consistent in the phase-field part.

2. Sharp-interface model

The reference equations for the problem of dendritic growth from a supercooled melt in presence of external fluid flow are those of the sharp-interface model

$$u_t + \mathbf{U}\nabla u = D\nabla^2 u,$$

$$\mathbf{n} \cdot \mathbf{V} = D\mathbf{n} \cdot (\nabla u|_s - \nabla u|_\ell),$$

$$u_i = -d_0/R - \beta\mathbf{n} \cdot \mathbf{V}. \tag{1}$$

Here, $u = c_p(T - T_m)/L$ is the normalized temperature, D is the thermal diffusivity, $\mathbf{n}$ is the local normal to the liquid–solid interface, $d_0 = \gamma T_m c_p/L^2$ is the capillary length, β is the kinetic coefficient, and $\mathbf{V}$ is the interface velocity. Here, we restrict ourselves to the symmetric model with equal densities and thermal diffusivities of solid and liquid phases.

Equations for the fluid velocity $\mathbf{U}$ are continuity and Navier–Stokes equations together with the zero velocity boundary condition at the interface

$$\nabla \cdot \mathbf{U} = 0,$$

$$\mathbf{U}_t + \mathbf{U}\nabla\mathbf{U} = -\frac{\nabla P}{\rho} + \nu\nabla^2\mathbf{U},$$

$$\mathbf{U}_i = 0. \tag{2}$$

3. Method

A combined phase-field/lattice-Boltzmann scheme has been developed to simulate dendritic growth from a supercooled melt.

The scheme consists of three main parts:

1. Simulation of solidification is accomplished using the phase-field model of Karma and Rappel [1,6].
2. The flow of liquid is simulated by the standard LBGK method [7] with incorporated interactions with solid and thermal convection.
3. The conductive and convective heat transfer is simulated by a multicomponent LBE method similar to the one used in Ref. [8].

The second step (flow simulation) can be dropped out in the case of purely diffusional growth.

The phase-field model is written as

$$\begin{aligned}\tau(\theta)\psi_t &= (\psi - \lambda u(1 - \psi^2))(1 - \psi^2) + \nabla \cdot (W^2(\theta)\nabla\psi) \\ &\quad - \partial_x(W(\theta)W'(\theta)\psi_y) \\ &\quad + \partial_y(W(\theta)W'(\theta)\psi_x),\end{aligned}$$

$$u_t + \mathbf{U}\nabla u = D\nabla^2 u + \frac{1}{2}\frac{\partial h(\psi)}{\partial t}. \tag{3}$$

The value of phase-field variable $\psi = 1$ corresponds to the solid, $\psi = -1$ — to the liquid phase. Here, W is an anisotropic interface width, τ is a relaxation time, $\theta = \arctan(\psi_y/\psi_x)$ — the angle between the local interface normal and the X-axis. We used the simplest form $h(\psi) = \psi$.

Using asymptotic expansion, the equations of a sharp-interface model (1) can be derived [1] with following expressions for the capillary length and kinetic coefficient:

$$d_0(\theta) = \frac{I}{\lambda J}(W(\theta) + \partial_\theta^2 W(\theta)),$$

$$\beta(\theta) = \frac{I}{\lambda J}\frac{\tau(\theta)}{W(\theta)}\left(1 - \lambda\frac{K + JF}{2I}\frac{W^2(\theta)}{\tau(\theta)}\right).$$

In order to obtain zero kinetic coefficient, the following relations must be imposed [1,6]:

$$W = W_0 A(\theta), \quad \tau = \tau_0 A^2(\theta), \quad \lambda = \frac{2ID\tau_0}{(K + JF)W_0^2}.$$

For our choice of $h(\psi)$, the values of coefficients are $I = 2\sqrt{2}/3$, $J = 16/15$, $K = 0.13604$, and $F = \sqrt{2} \ln 2$ [1,6]. We used the anisotropy function

$$A(\theta) = 1 + \varepsilon \cos 4\theta.$$

Later on we assume $\tau_0 = 1$, $W_0 = 1$.

The equation for the phase-field ψ was discretized on a uniform spatial lattice with grid spacing $\Delta x = 0.4$, and it was solved using the explicit Euler method with time step Δt.

To simulate the flow of the liquid and the heat transport, we exploit the LBGK method (see Ref. [2]). It uses one-particle distribution functions f_k defined at nodes of a regular spatial lattice as main variables. Different k correspond to different velocities $\mathbf{c}_k$ from a fixed set. In the two-dimensional model used here, these velocities are $\mathbf{c}_0 = (0,0)$, $\mathbf{c}_k = (\cos((k-1)\pi/2), \sin((k-1)\pi/2))$ for $k = 1, \dots, 4$, and $\mathbf{c}_k = \sqrt{2}(\cos((k-1/2)\pi/2), \sin((k-1/2)\pi/2))$ for $k = 5, \dots, 8$. Nonzero velocities point to neighbour and next-neighbour sites of a square lattice. The evolution equation for f_k is

$$f_k(t + \Delta t, \mathbf{x} + \mathbf{c}_k\Delta t) = f_k(t, \mathbf{x}) + \frac{f_k^{\mathrm{eq}} - f_k}{\tau_f}. \quad (4)$$

Equilibrium distribution functions f_k^{eq} depend on local fluid density $\rho = \sum_k f_k$ and velocity $\mathbf{U} = \sum_k f_k \mathbf{c}_k/\rho$ so that to ensure mass and momentum conservation and to provide the correct form of the momentum flux tensor [2,7].

Performing Chapman–Enskog expansion, one can derive from Eq. (4) the continuity and Navier–Stokes equations [2], with kinematic viscosity $v = (\tau_f - 1/2)/3$. The isothermal sound velocity is $c_s = 1/\sqrt{3}$, for small flow velocities the fluid is almost incompressible (effects of compressibility are proportional to U^2/c_s^2).

The influence of the growing pattern on the fluid flow was simulated as proposed in Refs. [9,10]. An additional dissipative force was introduced in partially filled regions

$$\mathbf{F}_{\mathrm{d}} = -v\frac{2h\phi^2}{W_0^2}\mathbf{U},$$

where $\mathbf{U}$ is the velocity of liquid, $h = 2.757$, $\phi = (1 + \psi)/2$ is the solid fraction. This provides correct velocity boundary condition at the diffuse interface.

Also, thermal convection in the liquid can be easily included introducing the buoyancy force $\mathbf{F}_{\mathrm{c}} = -\rho\alpha(1 - \phi)(T - T_0)\mathbf{g}$, with α — the thermal expansion coefficient, $\mathbf{g}$ — the gravity acceleration.

Action of forces on a liquid was simulated by the exact difference method of Ref. [11].

The temperature transport was simulated using a second set of distribution functions N_k. The evolution equation for them is

$$N_k(t + \Delta t, \mathbf{x} + \mathbf{c}_k\Delta t) = N_k(t, \mathbf{x}) + \frac{N_k^{\mathrm{eq}} - N_k}{\tau_T}.$$

Here, $N_k^{\mathrm{eq}} = N_k^{\mathrm{eq}}(T, \mathbf{U} + \Delta\mathbf{U}/2)$, where $T = \sum_k N_k$, $\mathbf{U} = \sum_k f_k \mathbf{c}_k/\sum_k f_k$, $\Delta\mathbf{U} = \mathbf{F}/\sum_k f_k$, $\mathbf{F} = \mathbf{F}_{\mathrm{d}} + \mathbf{F}_{\mathrm{c}}$ is the total force. This scheme leads to

$$\frac{\partial T}{\partial t} + \mathbf{U}\nabla T = \chi\nabla^2 T,$$

the equation for the convective and conductive heat transport with constant thermal diffusivity $\chi = (\tau_T - 1/2)/3$ (hence, the symmetric model was used).

In the LBE part of simulations, time and lattice step are usually assumed to be equal to one. To accommodate the solution of Eq. (3), the relaxation time should be $\tau_T = 1/2 + 3D\Delta t/\Delta x^2$, where D is the thermal diffusivity.

When the values of T become small, the scheme works poorly, therefore, we used $T = u + \Delta + 1.0$, where $\Delta = c_p(T_{\mathrm{m}} - T_0)/L$ is non-dimensional initial undercooling.

Comparing with the four-dimensional scheme of Miller et al. [3–5], our model is less computationally demanding and seems to be more suitable in 2D simulations.

We simulated the growth of a single needle crystal into the supercooled melt for some sets of anisotropy and supercooling values listed in

Ref. [1], and verified that our code yields the same tip velocities.

4. Pattern growth in a shear flow

We investigated the growth of a pattern into a horizontal shear flow near the solid wall. A small seed was initially placed at the centre of the bottom wall of the computational box. The boundary conditions for the phase-field equation were reflective at the bottom, $\psi = -1$ in the inflow and at the outer boundary, and $\partial\psi/\partial x = 0$ in the outflow. The boundary conditions for the flow were $\mathbf{U}_y = 0$ at the bottom, $\partial\mathbf{U}/\partial x = 0$ in the in- and outflow, $U_x = U_0$, $U_y = 0$ at the top boundary, $T = T_0$ in the inflow and at the top boundary, $\partial T/\partial y = 0$ at the bottom, and $\partial T/\partial x = 0$ in the outflow.

Results for non-dimensional initial undercooling $\Delta = 0.7, 15\varepsilon = 0.15, D = 3, \Delta t = 0.01, v = \frac{1}{3}$, $d_0 = 0.185$ and different fluid velocities are shown in Fig. 1. Contours present the boundary of growing patterns (points with $\psi = 0$) for times up to $t = 1400$, the time difference between contours is 50. Grid size 2001×1000. The reduced flow velocity is $\overline{U} = Ud_0\Delta x/D\Delta t$. In this case, the shape of the growing pattern was dendritic. Shear flow lead to enhanced growth of sidebranches at the upstream side. The direction of the arm perpendicular to the flow was only slightly modified.

Increasing the initial undercooling Δ to 0.8 we obtained a seaweed pattern (Fig. 2) which consists of doublons as main building blocks. Boundary contours are shown for times up to $t = 460$ with increments of 20. In this case, the presence of flow modified the growth direction significantly, the perpendicular arm bent upstream and became finally parallel to the flow.

5. Influence of parallel flow on the growth

The needles grown in the test computations were used as the initial configurations. The values of temperature and the phase field of single dendrites grown without flow were loaded.
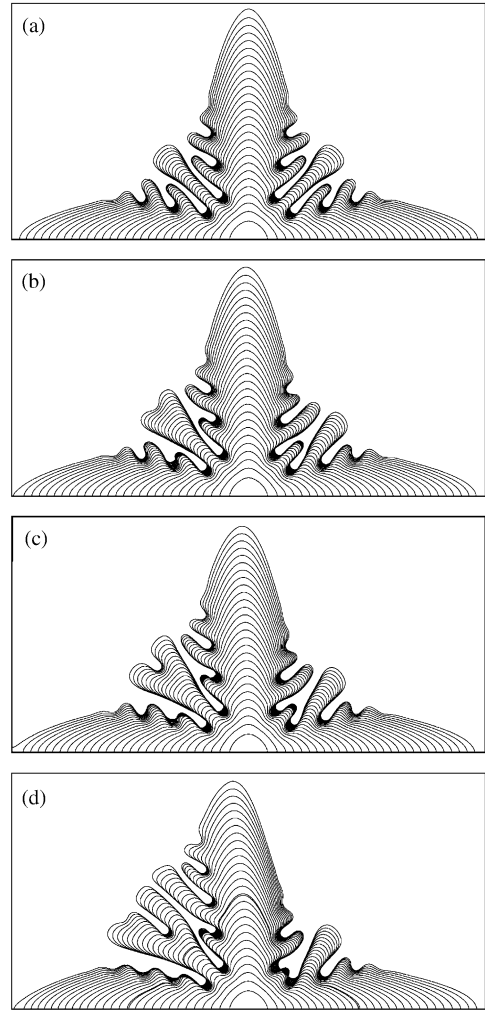
Fig. 1. Dendrite in a shear flow. Inflow from the left. Reduced velocity $\overline{U} = 0$ (a), $\overline{U} = 0.0123$ (b), $\overline{U} = 0.0247$ (c) and $\overline{U} = 0.0493$ (d).

Then the flow was initialized. Boundary conditions for the flow were constant flow velocity perpendicular to the upper boundary and zero velocity (and pressure) gradients at the lower boundary, with reflecting side boundaries. The flow evolved with a fixed configuration of the solid, and the relative velocity error was calculated at each time step as

$$U_{\mathrm{err}} = \frac{\sum |\hat{U}_x - U_x| + |\hat{U}_y - U_y|}{\sum |U_x| + |U_y|}.$$

(a)

(b)

(c)

(d)
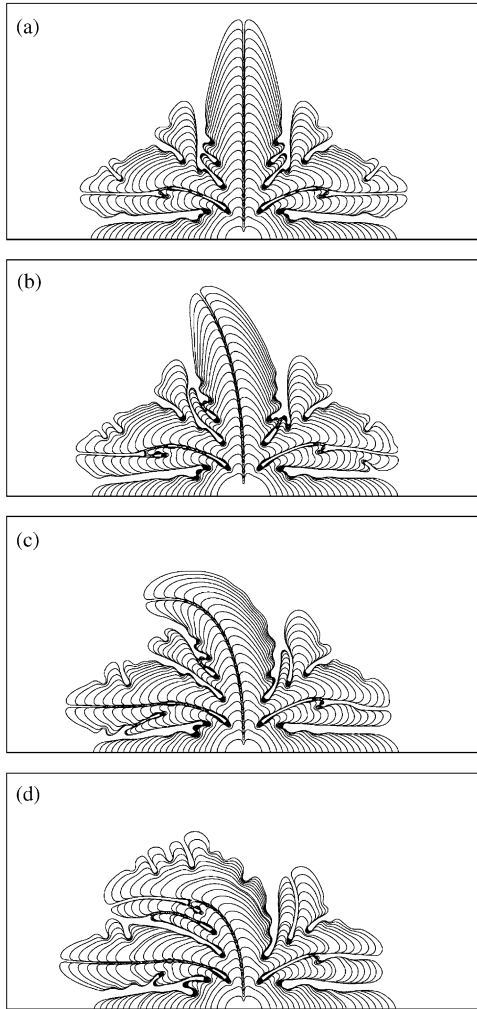
Fig. 2. Seaweed in a shear flow. Inflow from the left. Reduced velocity $\overline{U} = 0$ (a), $\overline{U} = 0.0247$ (b), $\overline{U} = 0.0493$ (c) and $\overline{U} = 0.0987$ (d).

Here, $\hat{\mathbf{U}}$ was the flow velocity at current time step, $\mathbf{U}$ — at the previous one, summation was over all grid nodes. The convergence condition was $U_{err} \leqslant 10^{-5}$. Then growth of the pattern was switched on and proceeded until convergence of the growth velocity.

We investigated the growth of a single dendritic tip for three cases: (1) $\varDelta = 0.65, 15\varepsilon = 0.75, D = 1, d_0 = 0.554$; (2) $\varDelta = 0.45, 15\varepsilon = 0.75, D = 4, d_0 = 0.139$; and (3) $\varDelta = 0.7, 15\varepsilon = 0.15, D = 3, d_0 =$

0.185. The dependence of the reduced tip velocity $\overline{V} = Vd_0/D$ and selection parameter $\sigma = \overline{R}^2\overline{U}/2$ on the flow Reynolds number is shown in Fig. 3a (case 1), and Fig. 4a (case 2). The behaviour of reduced tip radius $\overline{R} = R/d_0$ is shown in Figs. 3b, and 4b.

Dendrite tip velocity increases with the increase of flow velocity, whereas tip radius decreases. In the case of large anisotropy (Figs. 3 and 4), the selection parameter σ remains almost constant in some range of flow velocities. For small under-cooling ($\varDelta = 0.45$), the dependence of dendrite tip velocity can be fitted as $\overline{V} \sim \overline{U}^{0.38}$, dependence of tip radius as $\overline{\rho} \sim \overline{U}^{-0.16}$.

At large flow velocities, oscillations of the tip velocity were observed in case 3, accompanied by enhanced growth of side branches (see Fig. 5).
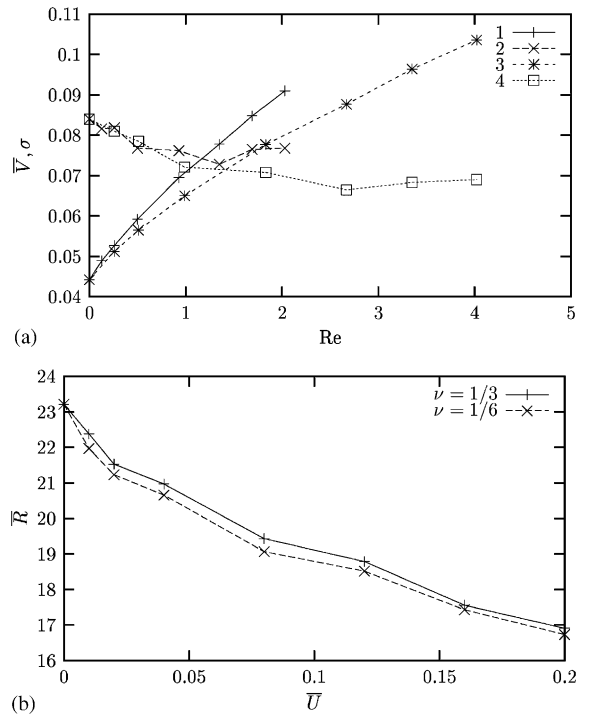
Fig. 3. $\varDelta = 0.65$, $15\varepsilon = 0.75$. (a) Dependence of reduced velocity $\overline{V}$ and selection parameter σ on flow Reynolds number. 1—$\overline{V}, \nu = \frac{1}{3}$; 2—$\sigma, \nu = \frac{1}{3}$; 3—$\overline{V}, \nu = \frac{1}{6}$; 4—$\sigma, \nu = \frac{1}{6}$. (b) Dependence of reduced tip radius $\overline{\rho}$ on reduced flow velocity $\overline{U}$.

(a)

(b)
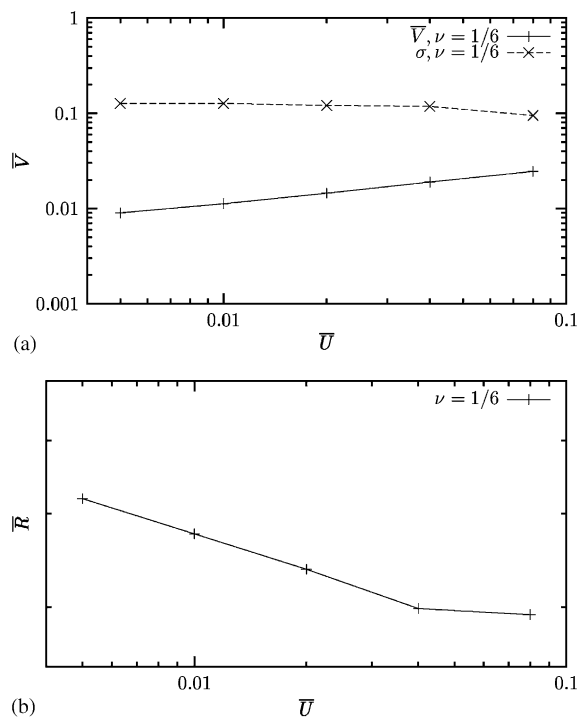
Fig. 4. $\varDelta = 0.45$, $15\varepsilon = 0.75$. (a) Dependence of reduced velocity $\overline{V}$ and selection parameter σ on flow Reynolds number. (b) Dependence of reduced tip radius $\overline{\rho}$ on reduced flow velocity $\overline{U}$.

Fig. 5. Growth of side branches, $\varDelta = 0.7$, $15\varepsilon = 0.15$. Reduced flow velocity $\overline{U} = 0.01$ (a) and $\overline{U} = 0.04$ (b).

6. Conclusions

We present an LB model for simulation of dendritic growth which incorporates naturally fluid flows and thermal convection. The method is sufficiently simple and effective.

The simulations showed a strong influence of the external flow on seaweed growth, in contrast with dendritic growth (Figs. 1 and 2).

The influence of parallel flow on the operating state of dendrite tip was investigated quantitatively (Figs. 3 and 4).

Our simulations have demonstrated the onset of tip velocity oscillations and enhancement of side-branching under parallel flow (Fig. 5).

References

[1] A. Karma, W.-J. Rappel, Phys. Rev. E 57 (1998) 4323.
[2] S. Chen, G. -Doolen, Ann. Rev. Fluid Mech. 30 (1998) 329.
[3] W. Miller, S. Succi, D. Mansutti, Phys. Rev. Lett. 86 (2001) 3578.
[4] W. Miller, S. Succi, J. Statist. Phys. 107 (2002) 173.
[5] W. Miller, Int. J. Mod. Phys. B 17 (2003) 227.
[6] A. Karma, W.-J. Rappel, Phys. Rev. E 53 (1996) R3017.
[7] Y.H. Qian, D. d'Humières, P. Lallemand, Europhys. Lett. 17 (1992) 479.
[8] X. Shan, Phys. Rev. E 55 (1997) 2780.
[9] C. Beckermann, H.-J. Diepers, I. Steinbach, A. Karma, X. Tong, J. Comp. Phys. 154 (1999) 468.
[10] X. Tong, C. Beckermann, A. Karma, Q. Li, Phys. Rev. E 63 (2001) 061601.
[11] A.L. Kupershtokh, Proceedings of the Seventh International Conference on Modern Problems of Electrophysics and Electrohydrodynamics of Liquids, St. Petersburg, Russia, 2003, p. 152.